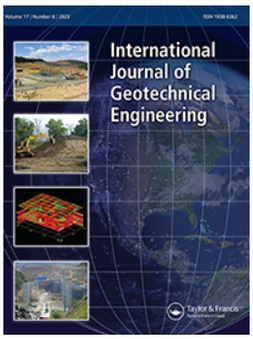

International Journal of Geotechnical Engineering

ISSN: (Print) (Online) Journal homepage: www.tandfonline.com/journals/yjge20

Use of in-situ tests like flat plate dilatometer (DMT) andSeismic Dilatometer (SDMT) vis-à-vis finite element-based software to examine the efficacy of ground improvement work at a high rise residential project in Kolkata

Kaustav Das, Shivam Bandyopadhyay & Kaushik Bandyopadhyay

To cite this article: Kaustav Das, Shivam Bandyopadhyay & Kaushik Bandyopadhyay (24 Jul 2024): Use of in-situ tests like flat plate dilatometer (DMT) andSeismic Dilatometer (SDMT) vis-à-vis finite element-based software to examine the efficacy of ground improvement work at a high rise residential project in Kolkata, International Journal of Geotechnical Engineering, DOI: 10.1080/19386362.2024.2377457

To link to this article: https://doi.org/10.1080/19386362.2024.2377457

INTERNATIONAL JOURNAL OF GEOTECHNICAL ENGINEERING
https://doi.org/10.1080/19386362.2024.2377457

Use of in-situ tests like flat plate dilatometer (DMT) andSeismic Dilatometer (SDMT) vis-à-vis finite element-based software to examine the efficacy of ground improvement work at a high rise residential project in Kolkata

Kaustav Das[a], Shivam Bandyopadhyay[b] and Kaushik Bandyopadhyay[a]

[a]Department of Construction Engineering, Jadavpur University, Kolkata, India; [b]Department of Civil Engineering, Meghnad Saha Institute of Technology, Kolkata, India

ABSTRACT

Rapid urbanization in India, particularly in Kolkata, has led to a scarcity of suitable land, necessitating effective ground improvement techniques. A case study was evaluated using 500mm diameter, 10m long plain cement concrete (PCC) piles installed at 2m c/c spacing to enhance subsoil for a high-rise residential structure. Initial Dilatometer (DMT) tests showed the subsoil was unsuitable for shallow foundations. Post-PCC piling, DMT tests revealed a 30-40% improvement in subsoil stiffness. The factor of Safety against liquefaction was calculated using DEEPSOIL software. Further analyses with DMT Settlement software and PLAXIS 2D confirmed that post-piling, the raft foundation settlement remained within permissible limits, proving the effectiveness of the ground improvement measures.

ARTICLE HISTORY
Received 15 September 2023
Accepted 30 June 2024

KEYWORDS
DMT/SDMT; pcc piling; *PGA*; DEEPSOIL; DMT settlement software; PLAXIS 2D

1. Introduction

The construction industry in India is experiencing rapid growth, leading to a surge in the construction of high-rise buildings. In certain regions of India, the presence of soft cohesive or loose cohesionless soil layers requires the use of deeper foundations and specialized techniques for the construction of these tall structures (Bandyopadhyay et al. 2021; Govindaraju and Bhattacharya 2012) and (Shiuly and Narayan 2012).

Geotechnical engineers often opt for driven piles to establish the substructures of various civil engineering projects, such as high-rise buildings, bridges, elevated water tanks, and dams. This choice is particularly common when dealing with upper ground layers consisting of soft clay or loose sand (Acharyya 2023). For Pile driving different types of hammer (i.e. drop, single-acting, double-acting, and diesel) are used as per Bureau of Indian Standards (IS 6426 1972).

Several studies have delved into various aspects of driven pile behaviour and performance. They observed changes in pore water pressure during pile driving and over time, along with variations in shaft and end resistance (Hanna 1967; Mabsout, Reese, and Tassoulas 1995). Other researchers examined skin friction using blow count data and the 1D wave propagation concept, presenting results on skin friction under various conditions (L. Zhang, Tang, and Ng 2001; L. M. Zhang et al. 2006). Researchers also focused on settlement characteristics in soft clay around piles, incorporating excess pore pressure variations into their analyses (Ali et al. 2011; Klammler et al. 2013; Zhao, Leng, and Zheng 2013). Furthermore, authors investigated the long-term load-carrying capacity of driven piles, noting an increase over time due to dissipation of excess pore water pressure (Alawneh and Sharo 2020; Yin et al. 2023; Y. Zhang et al. 2023).

During in-situ soil exploration at a residential project site in Kolkata, consistent soil conditions were identified using both DMT and SDMT methods. The underlying stratum comprises loose cohesionless subsoil, which fails to offer sufficient support to the superstructure. Consequently, it became essential to enhance the stiffness characteristics of the subsoil. To address this, pcc piles with a diameter of 500 mm and a length of 10.0 m were installed at intervals of 2.0 m c/c distance.

This case study thoroughly examines the effectiveness of pcc piling in enhancing the ground's stiffness for a high-rise residential project. The authors conducted DMT and SDMT tests both before and after the completion of the ground improvement work involving pcc piling. The study analyzes the shear strength and compressibility characteristics of the subsoil pre and post pcc piling. In November 2021, a total of six DMT tests (DMT1 through DMT6) were performed at the site. Among these, an SDMT test was executed at DMT6 location test. Subsequently, an additional six DMT tests (DMT′1 through DMT′6) were conducted in May 2022, after pcc piling was carried out adjacent to the initial DMT test locations.

Based on the obtained geotechnical properties (Bandyopadhyay et al. 2022; S. Marchetti et al. 2001) and (S. Marchetti 1980), including the horizontal stress index (K_d), Young's modulus (E), shear wave velocity (Vs), modulus of subgrade reaction (k_s), and the factor of safety (FS)

CONTACT Kaustav Das kd3853@gmail.com Department of Construction Engineering, Jadavpur University, Plot No. 8, B-73-80, Salt Lake Bypass, LB Block, Sector 3, Bidhannagar, Kolkata, West Bengal 700106, India

against liquefaction, calculations were conducted both before and after pcc piling. The *FS* was determined based on specific subsoil layers and particular *PGA* values. Layer-specific PGAs were computed using the finite element-based software DEEPSOIL (Hashash et al. 2020). These geotechnical parameters, assessed before and after the implementation of pcc piling, were compared to evaluate the effectiveness of the ground improvement measures as per (Bryson and El Naggar 2013).

Additionally, two software applications – DMT Settlement software, PLAXIS 2D – were utilized to calculate the settlement of a raft foundation before and after the implementation of pcc piling at this project site under the specified structural load. Based on the test results and data interpretation, recommendations regarding the effectiveness of the ground improvement measures are provided.

2. Methodology

2.1. Flat Dilatometer Test/Seismic Flat Dilatometer Test (DMT/SDMT)

The Flat Dilatometer Test (DMT) was conducted to assess the shear strength parameters of the subsoil at 20 cm depth intervals (S. Marchetti et al. 2001). Using suggested correlations (S. Marchetti et al. 2001) and the SDMT Elab software accompanying the equipment (Bandyopadhyay et al. 2022; S. Marchetti 1980; S. Marchetti et al. 2001) and (S. Marchetti 1997), parameters such as the angle of internal friction (ϕ), vertical drained constrained modulus (M_{DMT}), and Young's modulus (E) were determined at each 20 cm depth increment.

When employing the seismic probe in conjunction with the Dilatometer blade, known as SDMT, the shear modulus (G_0) can be directly derived from field V_s values obtained from shear wave velocity tests. Additionally, the V_s can be measured by integrating a seismic module into the DMT control box using the SDMT Elab software (Bandyopadhyay et al. 2022; S. Marchetti et al. 2001) and (D. M. T. Marchetti 0000).

2.2. Liquefaction analysis

The results from all DMT probes indicate that the subsoil beneath the raft foundation predominantly consists of sandy material. According to recent guidelines (Indian Standard 2016), it is recommended to conduct a comprehensive liquefaction analysis to assess the factor of safety against liquefaction across various sand layers.

The liquefaction analysis of the subsoil was performed using geotechnical parameters derived from the DMT tests conducted both before and after the pcc piling. The cyclic stress ratio (*CSR*) was computed as specified in (Indian Standard 2016) (Annexure F, Clauses (Shiuly and Narayan 2012) (Klammler et al. 2013), and (Hanna 1967) (Shiuly and Narayan 2012). (IS 6426 1972). (Shiuly and Narayan 2012)], with the detailed equation for its calculation provided as equation 1 in (Indian Standard 2016). Similarly, the cyclic resistance ratio (*CRR*) was determined following guidelines (Halder et al. 2022; Monaco et al. 2005) and (Kaushik and Bhattacharjee 2015), and the detailed equation for its calculation is presented as equation 2.

$$CSR = 0.65\left(\frac{a_{\max}}{g}\right)\left(\frac{\sigma v_0}{\sigma' v_0}\right) rd \quad (1)$$

Where,

$a_{\max}$ = peak ground acceleration (*PGA*) preferably in terms of g

g = acceleration due to gravity

σv_0 = vertical overburden stress

σ'_{v_0} = effective vertical overburden stress

r_d = stress reduction factor

$= 1 - 0.00765z (0 \le z \le 9.15m)$

$= 1.174 - 0.0267z (9.15 \le z \le 23.0m)$

($z$is the depth in metre below the ground surface)

If the *PGA* value is unavailable, $\left(\frac{a_{\max}}{g}\right)$ the ratio can be determined based on the seismic zone factor (Z) as outlined in Table 3 of (Indian Standard 2016). In this study, the finite element-based software DEEPSOIL was utilized to determine layer-specific *PGA* values. These obtained *PGA* values were then employed in the calculation of *CSR*.

$$CRR = 0.0107K_d^3 - 0.0741K_d^2 + 0.2169K_d - 0.1306$$

Where,

K_d = horizontal stress index = $\left(\frac{p_o - u_0}{\sigma'_{v0}}\right)$, where p_0 = corrected first reading of the DMT test, and u_0 = pre-insertion pore pressure.

Using equations 1 and 2, the factor of safety against initial liquefaction (*FS*) was determined as the ratio of *CRR* to *CSR*, expressed as $FS = \left(\frac{CRR}{CSR}\right)$. If the calculated *FS*value is less than 1, it indicates that the subsoil is susceptible to liquefaction [Indian Standard 2016, Annexure F].

2.3. DEEPSOIL

DEEPSOIL is a one-dimensional seismic site response software (Hashash et al. 2020) designed to offer layer-specific seismic responses of the subsoil. This is achieved based on input parameters such as V_s (shear wave velocity), the unit weight of the subsoil (γ), and earthquake motion data. In this study, the values of V_s and γ for the subsoil were derived from the SDMT results obtained at the DMT6 test location are used as input parameters.

2.4. Modulus of subgrade reaction (k_s)

The modulus of subgrade reaction (k_s) represents a theoretical relationship between soil pressure (q) and deflection (δ) and is utilized for foundation structural analysis (Bowels 1997). Typically, the modulus of subgrade reaction (k_s) is determined by examining the load versus displacement graphs derived from a plate load test (Bowels 1997). However, in 1961, Vesić proposed that if plate load test data is not available, the modulus of subgrade reaction (k_s) can alternatively be computed from the stress-strain modulus (E_s). A comprehensive equation for calculating ks is provided as equation 3 in (Bowels 1997).

$$k_s = \frac{1}{mBE'_s I_s I_F} \tag{3}$$

Where,

m = number of corners contributing to the settlement (m = 4 for centre, m = 1 for corner)

B = width of the foundation

$$E'_s = \frac{(1-\mu^2)}{E_s}, \tag{3.1}$$

E_s = Young's modulus of the subsoil

μ = Poisson's ratio of the sub soil

I_s, I_1, I_2 (Steinbrenner influence factor)

$$I_s = I_1 + \left(\frac{1-2\mu}{1-\mu}\right) I_2 \tag{3.2}$$

These factors depend upon $H/B$and L/B ratio, H = depth of stress-strain influence for structural member considered as $5B$,

L = length of the foundation.

I_F = Depth influence factor

2.5. Settlement analysis

Numerical analyses were conducted using DMT settlement software, PLAXIS 2D to determine the theoretical settlement of a raft foundation measuring 24.0 m × 52.0 m × 0.750 m under a specified structural load of 400 kPa. This raft foundation is situated at a depth of 5.25 m below the existing ground level (E.G.L.). Geotechnical parameters derived from the DMT tests conducted before and after the pcc piling were utilized for the modelling process. The structural properties of the foundation were determined based on the material characteristics of concrete and steel rebar. For this analysis, it was assumed that M25 grade concrete and Ø 16 mm steel rebar would be employed in constructing the raft foundation.

3. Site investigation

In November 2021, a total of six DMT tests were carried out at the project site. These tests, labelled as DMT1 through DMT6 for this case study, were conducted prior to the installation of pcc piles as part of the ground improvement measures. The selection of these test

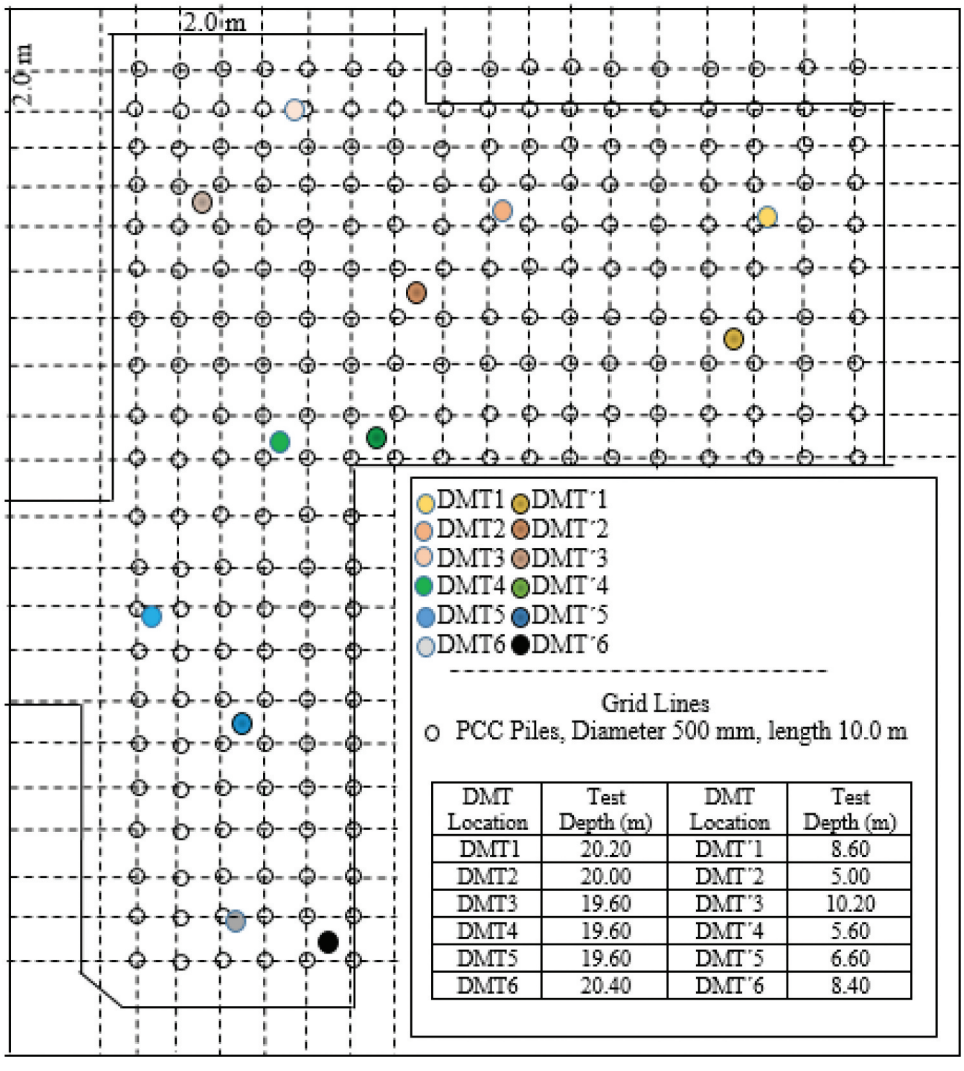

DMT Location	Test Depth (m)	DMT Location	Test Depth (m)
DMT1	20.20	DMT'1	8.60
DMT2	20.00	DMT'2	5.00
DMT3	19.60	DMT'3	10.20
DMT4	19.60	DMT'4	5.60
DMT5	19.60	DMT'5	6.60
DMT6	20.40	DMT'6	8.40

Figure 1. Site plan that for the test points and their depths, as well as the distribution of plain cement concrete pcc piles.

locations was influenced by the positioning of the towers: DMT1, DMT3, DMT4, and DMT6 were situated at the extremities of two towers, while DMT2 and DMT5 were positioned centrally between the towers (Figure 1).

Subsequently, in May 2022, an additional six DMT tests were performed adjacent to the original test points following the installation of pcc piles. These new test locations, referred to as DMT´1 through DMT´6 in this study, were situated approximately 3.5 metres away from their respective previous locations. Notably, these new test points were positioned centrally within a group of four pcc piles spaced at 2.0 metres centre-to-centre (Figure 1).

The geotechnical parameters derived from both sets of DMT tests indicate that the subsoil beneath the foundation level predominantly consists of sandy material, extending to the specified termination depth.

showcases the weighted average φ values collated from all DMT test sites, encompassing both pre and post pcc piling scenarios. Figure 3 provides a graphical representation illustrating the percentage increment in φ values subsequent to the pcc pile installation.

From Figure 2, it is evident that the angle of internal friction (φ) was determined up to an average depth of 6.0 m for the DMT test points following the installation of pcc piles. This limitation arose because the penetrometer, utilized to advance the DMT blade, reached its maximum capacity of 150 kN for penetration into the subsoil, achieving an average depth of 6.0 m post-pcc piling. Both Table 1 and Figure 3 indicate that there has been an enhancement in the φ value of the subsoil subsequent to the ground improvement work involving pcc piling. The primary factor contributing to this improvement is the densification of the subsoil resulting from the pcc piling,

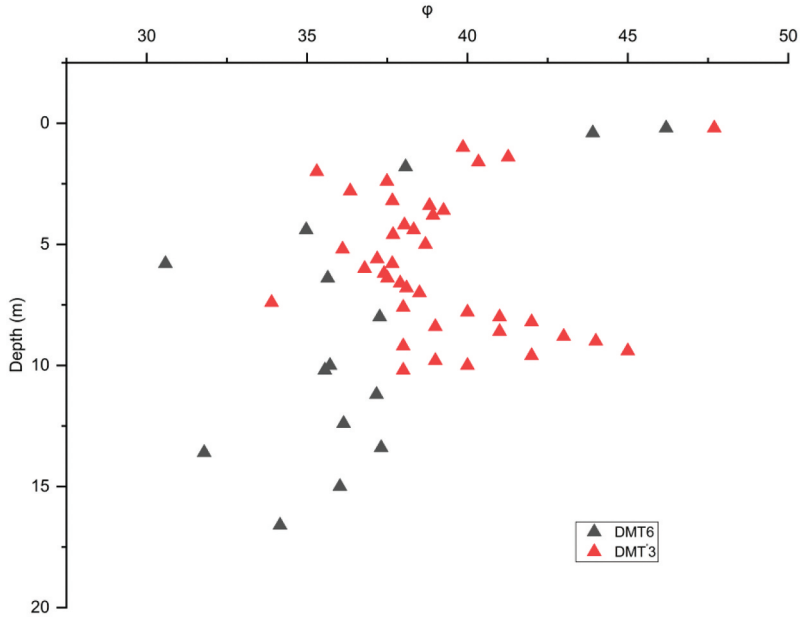

Figure 2. Variation of the angle of internal friction (φ) with depth for DMT6, DMT´3 test point.

Table 1. Average φ value.

Test Points	DMT1	DMT'1	DMT2	DMT'2	DMT3	DMT'3	DMT4	DMT'4	DMT5	DMT'5	DMT6	DMT'6
φ(◦)	35.4	37.5	36.4	40.2	36.5	39.5	34.7	39	33.9	38.6	35.2	39

4. Results and discussion

4.1. Angle of internal friction (φ)

At each designated test location, the angle of internal friction (φ) is ascertained using the standardized correlation advocated by (S. Marchetti et al. 2001). A comparative analysis is executed between the φ values extracted from the DMT tests performed before and after the implementation of pcc piles. Figure 2 delineates the depth-wise variation of φ, specifically focusing on the DMT test points DMT´3 and DMT6. Concurrently, Table 1

which consequently elevates the internal friction among the subsoil particles.

4.2. Vertical drained constrained modulus (M_{DMT})

According to reference (S. Marchetti et al. 2001), the constrained modulus (M) derived from the DMT test represents the vertical drained confined (one-dimensional) tangent modulus at σ'_{vo}. This modulus is analogous to the one obtained via

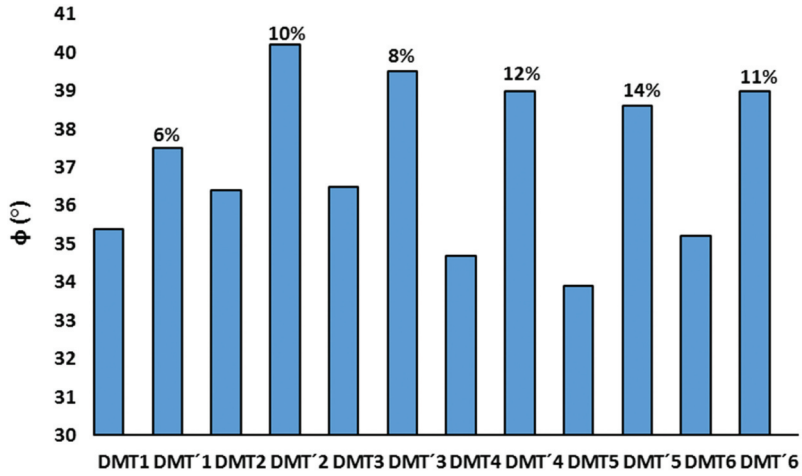

Figure 3. Percentage increment in φ values.

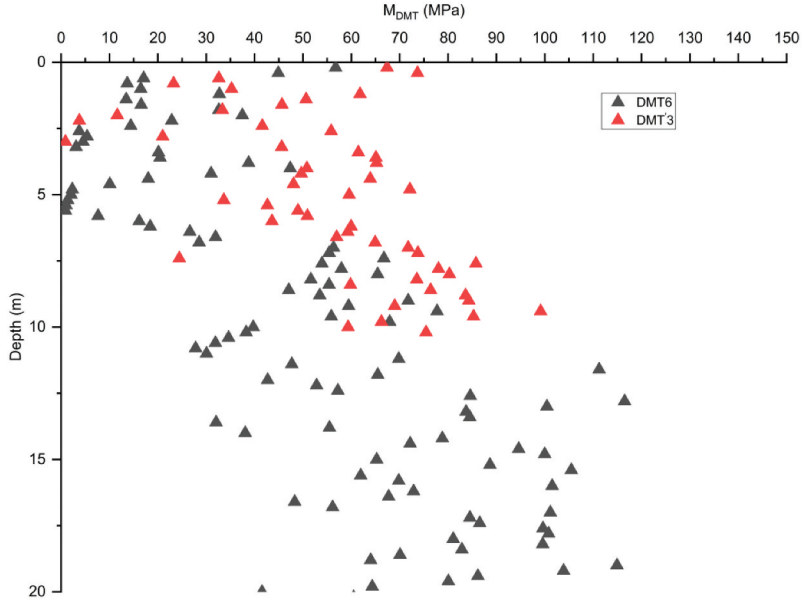

Figure 4. Variation of vertical drained constrained modulus (M_{DMT}) with depth for DMT´3 and DMT6 test point.

Table 2. Average M_{DMT} value.

Test Points	DMT1	DMT'1	DMT2	DMT'2	DMT3	DMT'3	DMT4	DMT'4	DMT5	DMT'5	DMT6	DMT'6
M_{DMT}(MPa)	33.9	41.8	35.1	67.3	27.4	55.8	21.3	40.4	22.1	43.6	19.1	45.1

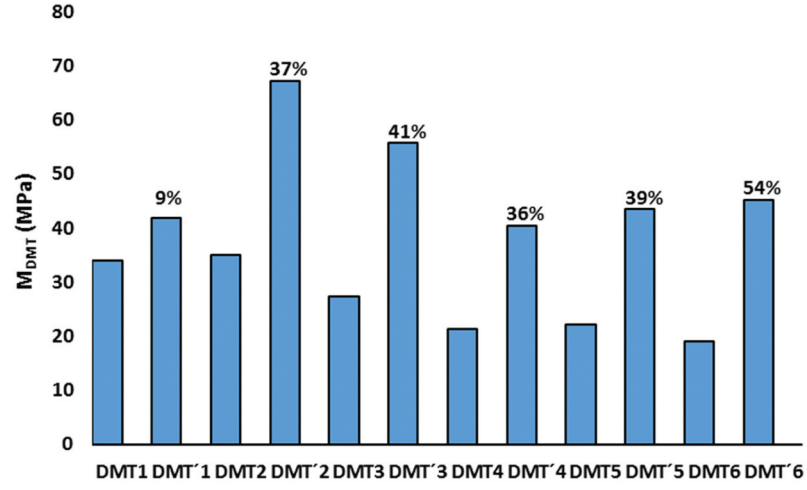

Figure 5. Percentage increment in M_{DMT} values.

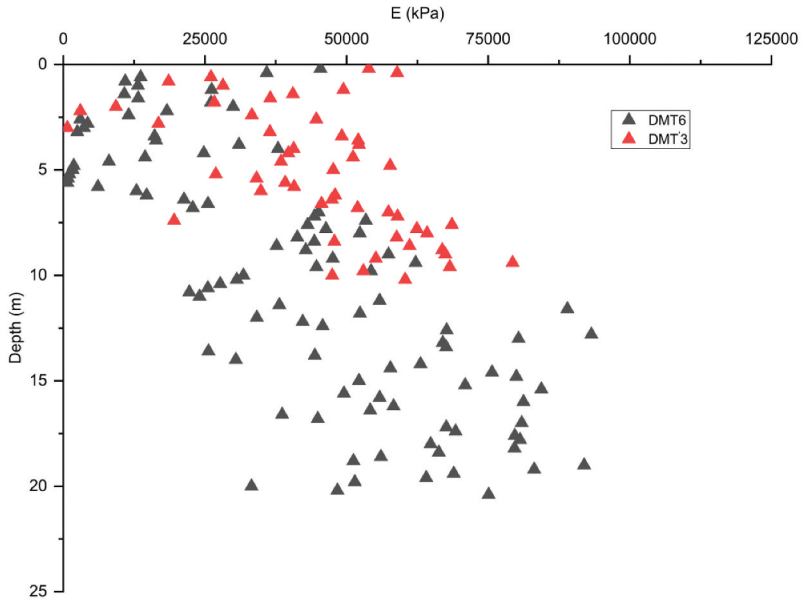

Figure 6. Variation of Modulus of Elasticity (*E*) with depth for DMT1, DMT´1, DMT2, DMT´2, DMT3, DMT´3 test point.

Table 3. Average *E* value.

Test Points	DMT1	DMT'1	DMT2	DMT'2	DMT3	DMT'3	DMT4	DMT'4	DMT5	DMT'5	DMT6	DMT'6
E (kPa)	27120	33440	28080	53840	21920	44640	17040	32320	17680	34880	15280	36080

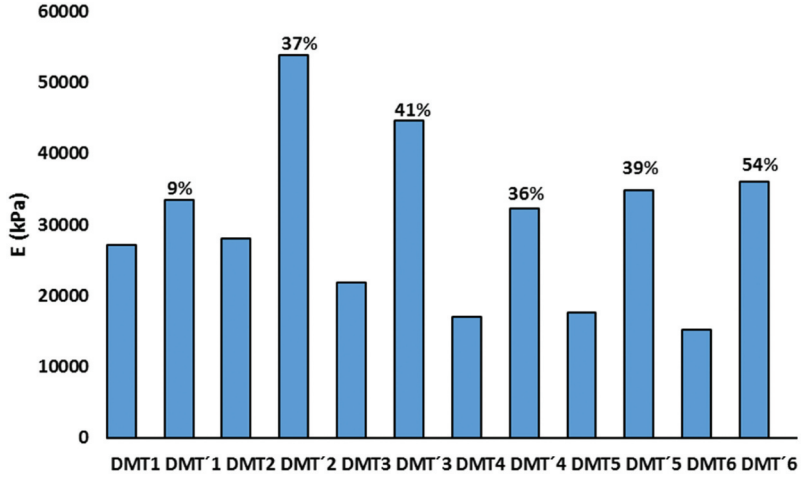

Figure 7. Percentage increment in *E* values.

oedometer tests, known as $E_{oed} = \frac{1}{m_v}$. Consequently, an augmentation in the M_{DMT} value indicates that the subsoil has exhibited increased stiffness and reduced compressibility.

The M_{DMT} values acquired from the DMT tests, both before and after pcc piling, were juxtaposed to discern any variations. Figure 4 delineates the depth-wise variation of M_{DMT} specifically for the DMT test points DMT´3 and DMT6. Concurrently, Table 2 presents the weighted average M_{DMT} values amalgamated from all DMT tests. Figure 5 provides a graphical representation illustrating the percentage increment in M_{DMT} values subsequent to the pcc pile installation.

From Figure 4 above, it can be noted that the depth-wise variation of M_{DMT} after pcc piling closely resembles that illustrated in the previous figure (Figure 2). Table 2, along with Figure 5, further indicates that the ground improvement measures have significantly mitigated the compressibility of the subsoil upto 30 to 40%. The primary contributing factor to this enhancement is the densification of the subsoil resulting from the pcc piling, which directly reduces the subsoil's compressibility.

Figure 8. SDMT test in progress at the project site.

Table 4. $V_s$and γ obtained from SDMT.

Depth (m)	γ(kN/m^3)
6.00	16
7.00	18
8.00	19
9.00	19
10.00	19
11.00	18
13.00	19
14.00	19
15.00	20
16.00	20
17.00	20
18.00	20
19.00	20
20.00	20

4.3. Modulus of elasticity (E)

The Modulus of Elasticity (E) for the subsoil can be directly determined from the vertical drained constrained modulus (M_{DMT}) using elasticity theory as referenced in (S. Marchetti et al. 2001). These parameters provide insights into the elastic characteristics of the subsoil. Figure 6 illustrates the depth-wise variation of E for the DMT locations, specifically DMT´3 and DMT6. Additionally, Table 3 presents the average E values derived from all DMT tests, while Figure 7 provides a graphical representation illustrating the percentage increment in E values subsequent to the pcc pile installation.

From Figure 6 above, it can be observed that the depth-wise variation of E exhibits similar characteristics to those depicted in the other two figures (Figures 2 and4). Table 3, along with Figure 7, further indicates that the E value of the subsoil has been enhanced upto 30 to 40% following the completion of the ground improvement work involving pcc piling. The primary reason for this improvement is the densification of the subsoil due to pcc piling, which elevates the Young's modulus of the subsoil.

4.4. Shear wave velocity (V_s) and unit weight (γ)

The shear wave velocity (V_s) and unit weight (γ) of the subsoil can be directly determined from the SDMT by incorporating a seismic module add-on to the DMT control box (Bandyopadhyay et al. 2022). Figure 8 illustrates the SDMT being conducted at the DMT6 test point.

The shear wave velocity is determined at intervals of 1.0 m below the foundation depth, while the unit weight (γ) of the subsoil is measured at 0.20 m depth intervals. Table 4 and Figure 9 display the layer-specific shear wave velocities (V_s) and the weighted average unit weight (γ) obtained from the SDMT.

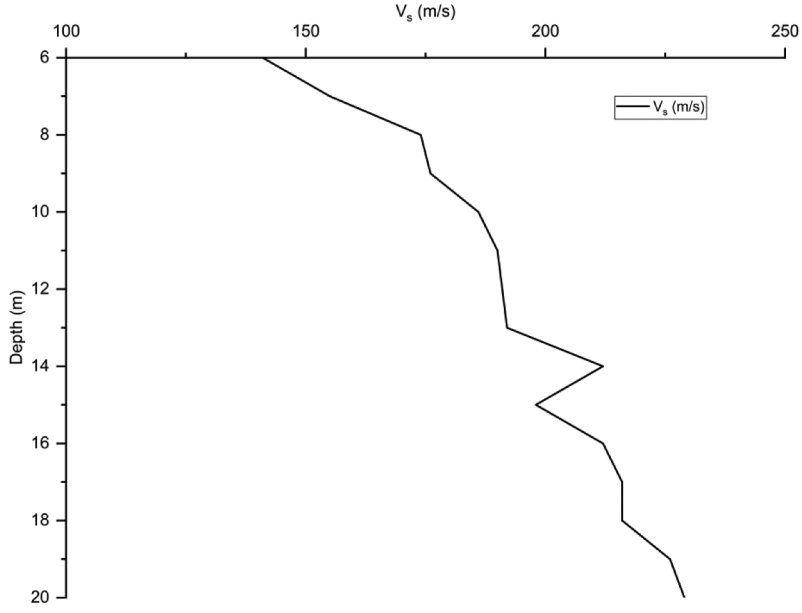

Figure 9. Variation of V_s with Depth at the testing location.

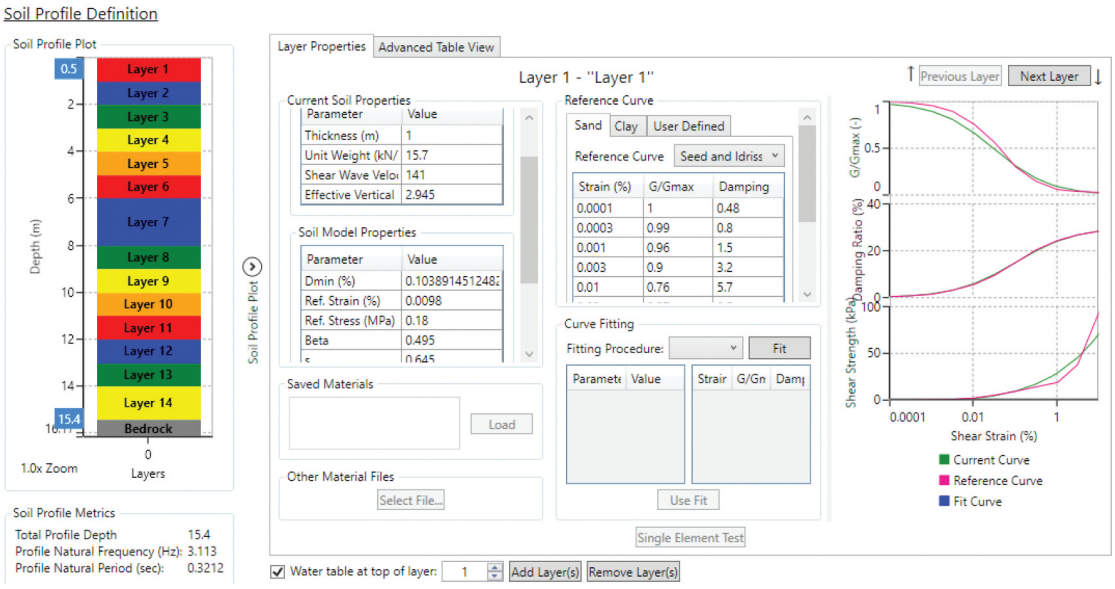

Figure 10. Subsoil layers in DEEPSOIL.

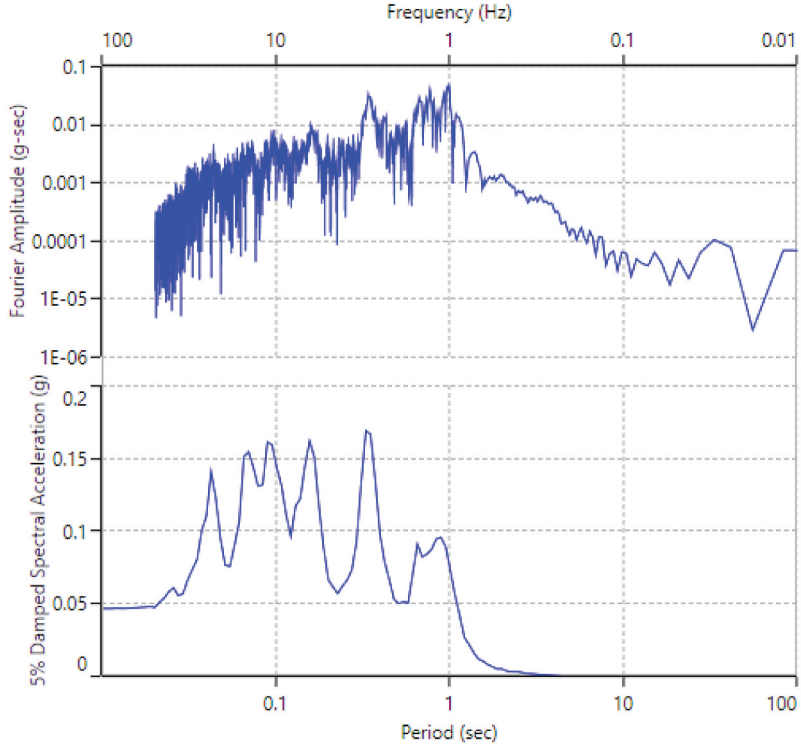

Figure 11. Response Spectrum of Nepal 2015 Earthquake.

4.5. Layer-wise PGA

The results derived from the SDMT, as presented in Table 4, serve as input parameters for DEEPSOIL for equivalent linear ground motion response analysis (ELRA) (Hashash et al. 2020). Figure 10 displays a sample input configuration for a subsoil layer. Given that the 2015 India-Nepal earthquake stands as the most significant earthquake in India over the past decade, its time history data, sourced from (NEIC), is utilized as the motion input within the software. Consequently, the data produces a response spectrum of the earthquake, as depicted in Figure 11.

Upon concluding the ELRA analysis, both the response spectrum and Peak Ground Acceleration (*PGA*) for each layer are determined. Figure 12 illustrates the response

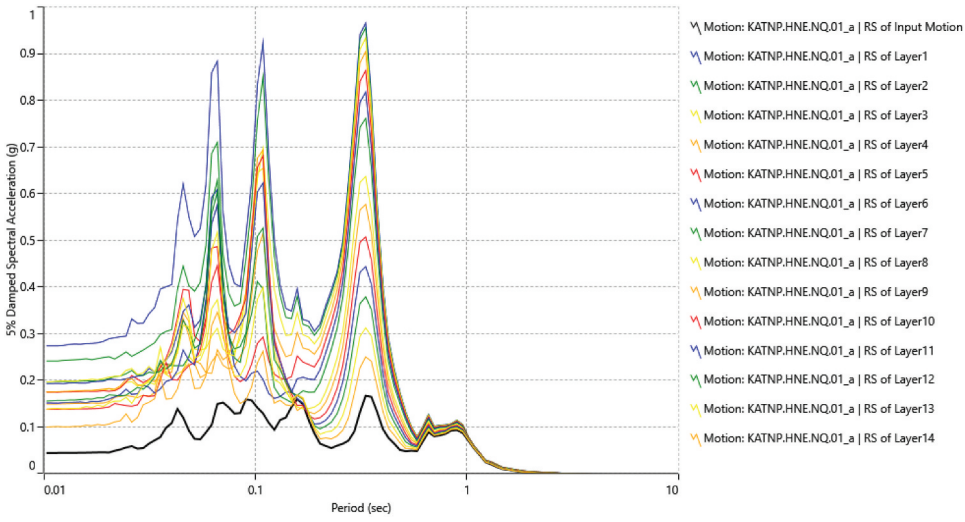

Figure 12. Subsoil layer wise response spectrums.

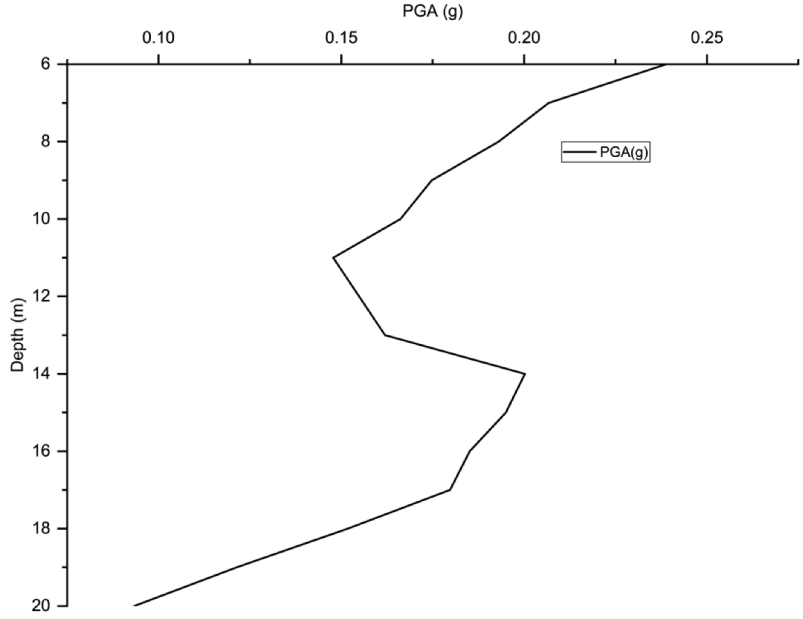

Figure 13. Variation of PGA.

Table 5. *PGA* obtained from DEEPSOIL analysis.

PGA (g)	
Depth (m)	*PGA* (g)
0	0.24
1	0.21
2	0.19
3	0.17
4	0.17
5	0.15
6	0.16
8	0.20
9	0.20
10	0.19
11	0.18
12	0.15
13	0.12
14	0.09

spectrum, while Figure 13 presents the *PGA* values for the individual layers.

4.6. Liquefaction analysis

Liquefaction analysis of the subsoil was conducted based on equations 1 and 2.

$$CSR = 0.65\left(\frac{a\,\max}{g}\right)\left(\frac{\sigma v0}{\sigma' v0}\right)rd \tag{1}$$

The *PGA* values $\left(\frac{a_{\max}}{g}\right)$ for each layer were derived from Table 5. The *CSR* was computed from a depth of 5.40 m beneath the existing ground level, given that the depth of the foundation is 5.25 m below the existing ground level. Geotechnical parameters from the SDMT6 and DMT′3 test

Table 6. Typical Computation of FS against liquefaction as per (Indian Standard 2016.).

SDMT6									
Depth below EGL, m	γ (kN/m^3)	r_d	σ_v (kPa)	σ_v' (kPa)	*CSR*	K_d	*CRR*	*FS*	Conclusion
5.40	14.7	0.96	79.46	67	0.20	2.5	0.12	0.58	Liquefiable
5.60	14.7	0.96	82.40	68	0.20	1.7	0.07	0.37	Liquefiable
5.80	16.7	0.96	96.73	69	0.24	1.5	0.07	0.28	Liquefiable
6.00	16.7	0.95	100.06	70	0.24	2.8	0.13	0.55	Liquefiable
6.20	16.7	0.95	103.40	71	0.21	3.1	0.15	0.71	Liquefiable
6.40	18.6	0.95	119.29	73	0.23	3.7	0.20	0.86	Liquefiable
6.60	17.7	0.95	116.54	74	0.22	4.6	0.34	1.54	Non Liquefiable
6.80	17.7	0.95	120.07	76	0.22	4.6	0.33	1.48	Non Liquefiable
7.00	19.1	0.95	133.91	78	0.24	6.1	0.85	3.47	Non Liquefiable
7.20	17.7	0.94	127.14	79	0.17	5.7	0.69	4.11	Non Liquefiable
7.40	19.1	0.94	141.56	81	0.18	7.0	1.40	7.70	Non Liquefiable
7.60	19.1	0.94	145.38	83	0.18	5.7	0.70	3.83	Non Liquefiable
7.80	19.1	0.94	149.21	85	0.18	6.1	0.88	4.78	Non Liquefiable
8.00	19.6	0.94	156.96	87	0.19	5.1	0.46	2.46	Non Liquefiable
8.20	19.1	0.94	156.86	89	0.15	5.6	0.64	4.22	Non Liquefiable
8.40	19.1	0.94	160.69	90	0.15	6.0	0.79	5.22	Non Liquefiable
8.60	17.7	0.93	151.86	92	0.14	5.0	0.44	3.17	Non Liquefiable
8.80	19.1	0.93	168.34	94	0.15	6.0	0.82	5.36	Non Liquefiable
9.00	19.1	0.93	172.17	96	0.15	6.6	1.13	7.39	Non Liquefiable
9.20	19.1	0.93	175.99	98	0.19	5.9	0.77	4.19	Non Liquefiable
9.40	19.1	0.92	179.82	99	0.18	7.2	1.59	8.60	Non Liquefiable
9.60	19.1	0.92	183.64	101	0.18	6.0	0.81	4.41	Non Liquefiable
9.80	19.1	0.91	187.47	103	0.18	6.2	0.90	4.94	Non Liquefiable
10.00	18.6	0.91	186.39	105	0.18	3.8	0.21	1.16	Non Liquefiable
10.20	18.6	0.90	190.12	107	0.20	3.7	0.19	0.98	Liquefiable
10.40	17.7	0.90	183.64	109	0.19	3.7	0.20	1.05	Non Liquefiable
10.60	17.7	0.89	187.17	110	0.19	3.4	0.17	0.93	Liquefiable
10.80	17.7	0.89	190.71	112	0.19	3.3	0.16	0.88	Liquefiable
11.00	17.7	0.88	194.24	113	0.19	3.1	0.15	0.80	Liquefiable

Table 7. Typical Computation of FS against liquefaction as per (Indian Standard 2016.).

DMT'3									
Depth below EGL, m	γ (kN/m^3)	r_d	σ_v (kPa)	σ_v'(kPa)	*CSR*	K_d	*CRR*	*FS*	Conclusion
5.40	17.7	0.96	95.35	68	0.24	5.3	0.55	2.32	Non Liquefiable
5.60	18.6	0.96	104.38	70	0.25	5.0	0.44	1.75	Non Liquefiable
5.80	18.6	0.96	108.11	72	0.25	5.5	0.60	2.37	Non Liquefiable
6.00	18.6	0.95	111.83	73	0.26	4.6	0.35	1.37	Non Liquefiable
6.20	18.6	0.95	115.56	75	0.22	5.2	0.51	2.31	Non Liquefiable
6.40	18.6	0.95	119.29	77	0.22	5.3	0.54	2.46	Non Liquefiable
6.60	18.6	0.95	123.02	79	0.22	5.8	0.71	3.21	Non Liquefiable
6.80	19.6	0.95	133.42	80	0.24	6.0	0.82	3.50	Non Liquefiable
7.00	19.6	0.95	137.34	82	0.24	6.5	1.11	4.69	Non Liquefiable
7.20	19.1	0.94	137.73	84	0.17	7.8	2.13	12.52	Non Liquefiable
7.40	18.6	0.94	137.93	86	0.17	8.1	2.43	14.55	Non Liquefiable
7.60	19.1	0.94	145.38	88	0.17	8.1	2.43	14.11	Non Liquefiable
7.80	19.1	0.94	149.21	90	0.17	7.5	1.85	10.74	Non Liquefiable
8.00	19.1	0.94	153.04	92	0.17	7.9	2.26	13.05	Non Liquefiable
8.20	19.1	0.94	156.86	94	0.14	6.5	1.06	7.44	Non Liquefiable
8.40	19.1	0.94	160.69	95	0.14	5.6	0.64	4.45	Non Liquefiable
8.60	19.1	0.93	164.51	97	0.14	6.2	0.90	6.28	Non Liquefiable
8.80	19.1	0.93	168.34	99	0.14	7.3	1.68	11.64	Non Liquefiable
9.00	19.1	0.93	172.17	101	0.14	8.1	2.45	16.94	Non Liquefiable
9.20	19.1	0.93	175.99	103	0.18	6.2	0.91	5.19	Non Liquefiable
9.40	19.1	0.92	179.82	105	0.18	8.5	2.93	16.73	Non Liquefiable
9.60	19.1	0.92	183.64	107	0.17	6.7	1.21	6.95	Non Liquefiable
9.80	19.1	0.91	187.47	108	0.17	5.7	0.67	3.85	Non Liquefiable
10.00	19.1	0.91	191.30	110	0.17	5.7	0.68	3.91	Non Liquefiable
10.20	19.1	0.90	195.12	112	0.19	6.2	0.93	4.78	Non Liquefiable

points were utilized for this analysis.Both the vertical overburden stress (σ_v) and the effective vertical overburden stress (σ'_v)were calculated at 20 cm depth intervals (S. Marchetti et al. 2001). The stress reduction factor (r_d)was determined in accordance with equations 1.1 and 1.2, considering the depth variations.

$$CRR = 0.0107K_d{}^3 - 0.0741K_d{}^2 + 0.2169K_d - 0.1306 \quad (2)$$

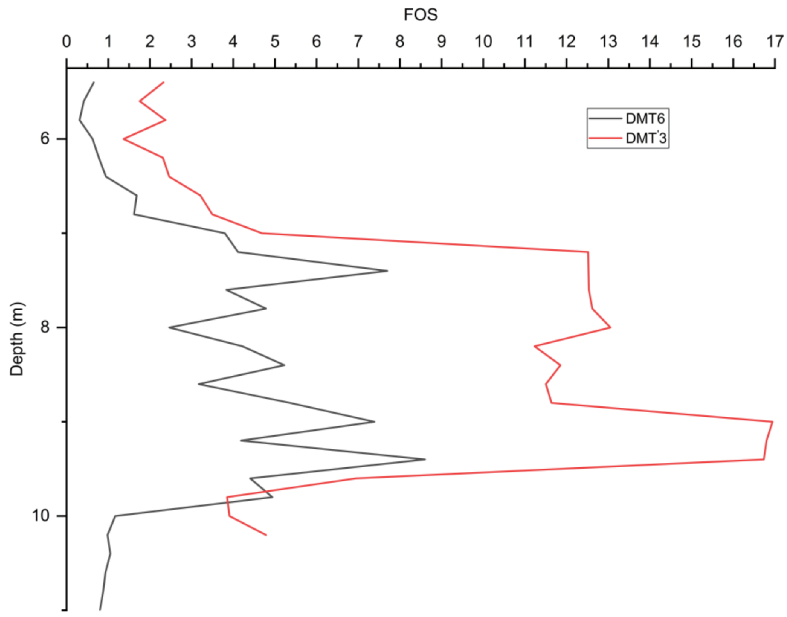

Figure 14. Variation of *FS* with depth at DMT6 and DMT′3 test point.

Table 8. Material properties of the sub soil before pcc piling.

Parameter	Name	Value	Unit
Material Model	Model	Mohr-Coulomb	-
Material Type	Type	Drained	-
Unit weight of soil above phreatic level	γ_{unsat}	16.2	kN/m^3
Unit weight of soil below phreatic level	γ_{sat}	18.2	kN/m^3
Young's Modulus of soil	E'	53.49E3	kN/m^2
Poisson's Ratio	ν'	0.30	-
Cohesion	C'_{ref}	0.001	kN/m^2
Friction Angle	φ'	30	°

Table 9. Material properties of the sub soil after pcc piling.

Parameter	Name	Value	Unit
Material Model	Model	Mohr-Coulomb	-
Material Type	Type	Drained	-
Unit weight of soil above phreatic level	γ_{unsat}	17	kN/m^3
Unit weight of soil below phreatic level	γ_{sat}	19	kN/m^3
Young's Modulus of soil	E'	54.40E3	kN/m^2
Poisson's Ratio	ν'	0.30	-
Cohesion	C'_{ref}	0.001	kN/m^2
Friction Angle	φ'	35	°

Table 10. Material properties of the raft (plate).

Parameter	Name	Value	Unit
Material Behaviour	Model	Elastic	-
Normal Stiffness	*EA*	8.65E6	kN/m
Flexural Rigidity	*EI*	4.06E5	kNm^2/m
Unit weight	*w*	18.75	kN/m/m
Poisson's Ratio	*v*	0.15	-

CRR calculations were based on the horizontal stress index (K_d) obtained from DMT tests at a depth of 5.40 m beneath the existing ground level, aligning with the foundation's position.

The factor of safety against initial liquefaction (*FS*) was computed as the quotient of *CRR* to *CSR*. Tables 6 and 7 detail the liquefaction analysis for the DMT6 and DMT′3 test points, respectively. Notably, the penetrometer could penetrate the subsoil to a depth of 10.20 m post the ground improvement work (pcc piling) at the DMT′3 test location. For consistent comparison, *FS* values were computed up to an average depth of 10.20 m. Figure 14 shows the variation of *FS* from the above Tables 6 and 7 with depth.

From the modified figure (Figure 12), it is evident that the factor of safety (*FS*) against liquefaction below the foundation level is less than 1 up to an average depth of 6.40 m, as well as between 10.0 m and 11.0 m prior to the ground improvement work. However, following the execution of the ground improvement measures (pcc piling), densification of the subsoil enhanced its resistance to cyclic loading. This improvement effectively minimized the risk of soil liquefaction, resulting in an increased Factor of Safety (*FS*) against liquefaction across all sand layers beneath the foundation, ensuring values surpassing 1.

4.7. Estimation of k_s

Utilizing equation 3, the modulus of subgrade reaction for a raft foundation measuring 24.0 m × 52.0 m was computed based on the geotechnical parameters of the subsoil derived from the DMT tests conducted at DMT6 and DMT′3 locations. Post the ground improvement work involving pcc piling, the penetrometer could access the subsoil up to an average depth of 11.0 m. In this analysis, the modulus of subgrade reaction (k_s) was determined, considering a depth of stress-strain influence (H) as 10.20 m to ensure consistent and accurate comparisons. The k_s values derived from the DMT6 and DMT′3 test points are 2.22E^6 and 3.31E^{6}kN/m respectively. For further details, see Appendix A.

Pcc piling mechanically densified and consolidated the adjacent subsoil, which augments the foundation's load-bearing capacity, minimizes settlement, and consequently elevates the k_s value upto 20%.

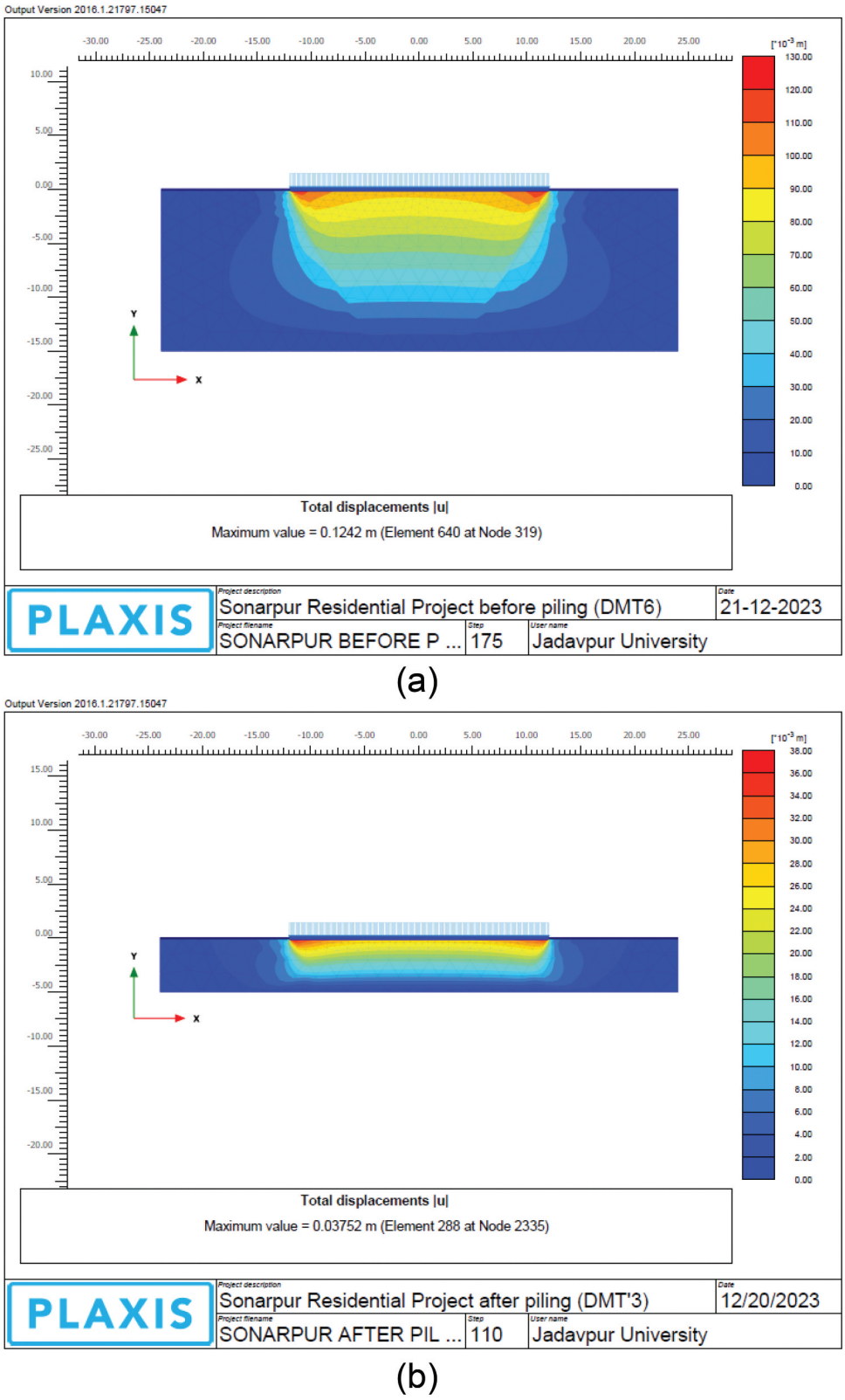

Figure 15. Numerical analysis result of the settlement of the raft foundation before the pcc piling.

4.8. Settlement analysis

For the settlement analysis of a raft foundation measuring 24.0 m × 52.0 m × 0.75 m and positioned 5.25 m below the existing ground level, several software tools were employed: DMT Settlement software, PLAXIS 2D. These tools facilitated a comprehensive evaluation against a specified structural load of 400 kPa.

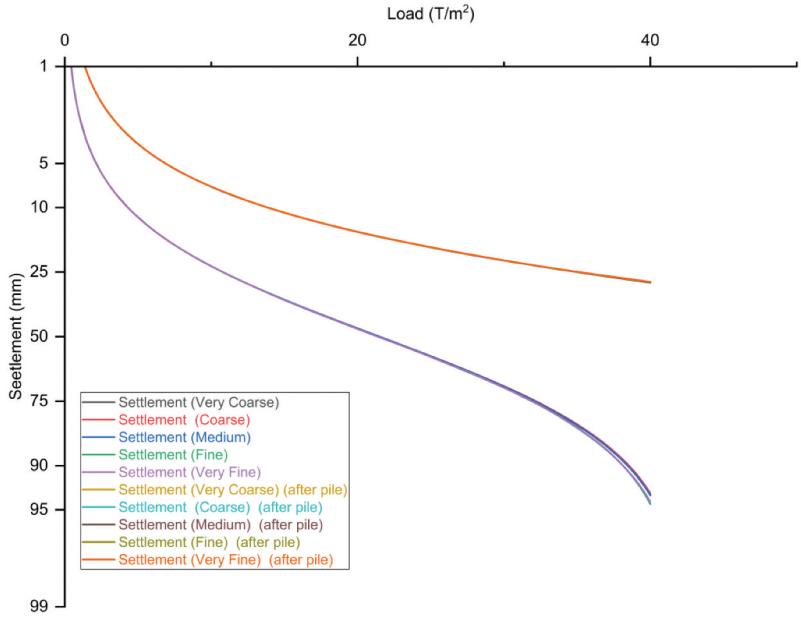

Figure 16. Variation of settlement with change in mesh size.

Table 11. Settlement analysis of the raft foundation at the test site.

Location	Size of foundation (m × m × m)	Depth of Foundation below E.G.L (m)	Suggested structural load (kPa)	Settlement (mm)	
				DMT Settlement Software	Plaxis
DMT6 (Before pcc piling)	24.0 × 52.0 × 0.75	5.25	400	116.0	124.2
DMT′ 3 (after pcc piling)				30.52	37.52

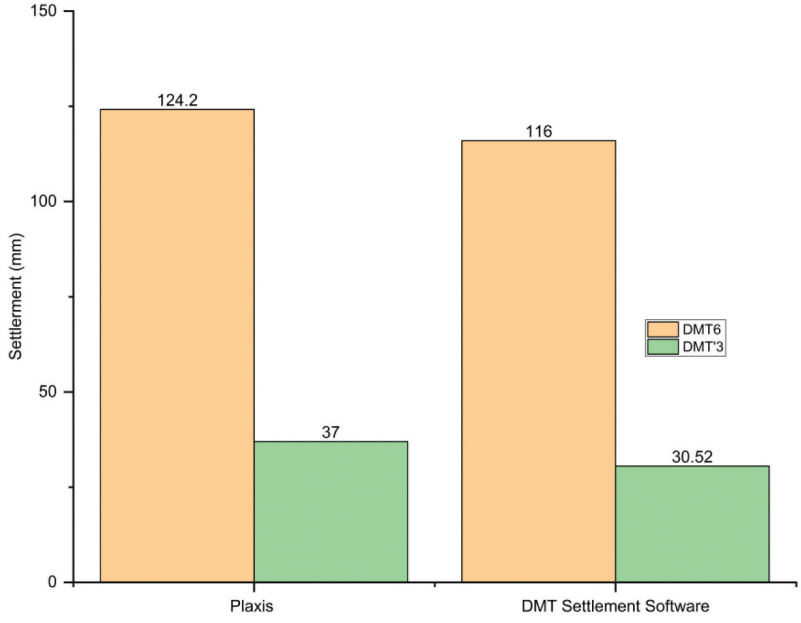

Figure 17. Settlement analysis of the raft foundation at the test site before and after pcc piling.

From a series of DMT tests conducted both pre and post pcc piling, the shear strength and compressibility parameters extracted from DMT6 and DMT′3 test locations were utilized for the subsequent finite element analysis (*FEA*).

The *FEA* was executed under plane strain conditions. This assumption postulates a scenario where the cross-section, extending indefinitely in the out-of-plane direction, remains consistent (NEIC, 0000). Tailoring the boundary conditions according to the raft foundation dimensions, the optimal settings were established as $2B$ (where B denotes the breadth of the foundation). The ranges for X_{max} and X_{min} span from 24.0 m to −24.0 m, while those for Y_{max} and Y_{min} oscillate between 70.0 m and 0.0 m.

Within the framework of PLAXIS 2D, the weighted average of shear strength and compressibility parameters of the subsoil was harnessed for modelling purposes. The reason for using PLAXIS 2D instead of PLAXIS 3D for finding settlement of shallow foundations lies in the use of considerable size (Bandyopadhyay et al. 2022) to the tune of 24.0 m × 52.0 m. For the raft material, the specifications assumed the utilization of M25 grade concrete. The determination of normal stiffness (EA) and flexural rigidity (EI) for the raft was achieved through calculations based on equations 4 and 5, as referenced in (Das et al. 2022; Ravichandran et al. 2021; Salahudeen and Sadeeq 2017; Vilas and Moniuddin 2015).

$$\mathrm{EA} = \frac{\mathrm{E} \times \mathrm{B} \times t}{L} \tag{4}$$

$$\mathrm{EI} = \frac{\mathrm{E} \times \mathrm{B} \times t^3}{12 \times L} \tag{5}$$

Where, E = Young's modulus of concrete = $5000\sqrt{f_{ck}}$, f_{ck} = compressive strength of concrete, here it is considered as 25 MPa, B = breadth of the foundation, t = thickness of the foundation.

Tables 8, 9 and table 10 present the material properties of both the subsoil and the raft within the PLAXIS 2D software, delineating the characteristics both before and after the implementation of pcc piling. Furthermore, Figure 15(a,b) display the results generated from PLAXIS 2D specifically at the DMT6 and DMT′3 test locations,

Ultimately, a finite element mesh is constructed for the model. Notably, the mesh quality exhibits an average maximum value of 1.00 and a minimum of 0.56 across both *FEA* instances. The load-settlement pattern is evaluated for different mesh configurations as shown in Figure 16. It is revealed that the identical load-settlement curves are obtained after fine mesh refinement. This indicates a relatively consistent mesh distribution, suggesting that the element sizes are appropriately chosen. Within the context of the *FEA*, the deformation boundaries are defined such that both the X_{max} and X_{min} boundaries are fixed horizontally. In contrast, the Y_{max} boundary is set to a free condition, while the Y_{min} boundary is completely fixed.

In the DMT Settlement software, the subsoil characteristics sourced from DMT6 and DMT3 test points are utilized. The settlement analysis conducted via this software adheres to the principles of one-dimensional consolidation theory (S. Marchetti et al. 2001). Table 11 presents the settlement analysis results for the raft foundation under a structural load of 400 kPa. Figure 17 presents the graphical representation of Table 11.

From Table 11 and Figure 17, it becomes evident that post-ground improvement work (pcc piling), the settlement values derived from DMT Settlement software and PLAXIS 2D have decreased by 70% compared to the values recorded before the ground improvement. Prior to the pcc piling, the settlement values from these software tools surpassed the allowable limits set by the relevant Bureau of Indian Standard (Indian Standard 2006). However, post pcc piling, the settlement values from these tools are comfortably within the permissible limits as stipulated by the Bureau of Indian Standard (Indian Standard 2006).

All settlement values derived from the numerical analysis align with those obtained from the principles of one-dimensional consolidation theory, thereby validating the finite element modelling approach. Notably, this analysis does not incorporate correction factors, e.g. Depth, rigidity etc.

The settlement of a foundation is intricately tied to the compressibility of the subsoil beneath it. When the subsoil becomes less compressible, it essentially means that it can withstand greater loads without undergoing significant deformation. This reduced compressibility leads to an increase in the stiffness or modulus of the subsoil, often denoted as the E value in geotechnical studies (Bandyopadhyay et al. 2022). The findings from the DMT tests depicted in Figures 3, 5, and figure 7 corroborate this understanding.

5. Conclusions

After an exhaustive evaluation of the shear strength and compressibility characteristics of the subsoil, both pre and post pcc piling, specific findings from this case study are summarized below:

- The application of pcc piling resulted in a notable enhancement by improving the subsoil's shear strength and compressibility by an estimated 30–40%.
- Post pcc piling interventions, there was a discernible improvement in the factors of safety against liquefaction, the modulus of subgrade reaction (k_s), and the settlement outcomes.
- The inclusion of site-specific Peak Ground Acceleration (PGA) values, tailored to reflect localized soil conditions and groundwater levels, played a crucial role. The obtained site-specific PGA of 0.24 g contrasts with the suggested value of 0.16 g (Indian Standard 2016). This incorporation of site-specific PGA renders the assessment of liquefaction susceptibility more accurate within the subsoil profile.
- The enhancements post ground improvement measures led to a substantial reduction approximately 70%—in settlement values, ensuring they remained within the accepted parameters delineated by the Bureau of Indian Standard (Indian Standard 2006).

- Conclusively, the synergy of in-situ tests like DMT/SDMT alongside advanced finite element software offers a robust methodology to assess and validate the effectiveness of ground improvement initiatives on-site.

Acknowledgments

The authors express their sincere thanks to Studio Prof. Marchetti s.r.l., Rome, Italy, and Pagani Geotechnical Equipment, Calendasco, Italy, BENTLEY EDUCATION for providing assistance at various stages for successful completion of the work.

Disclosure statement

No potential conflict of interest was reported by the author(s).

Informed Consent

Informed consent was obtained from all individual contributors involved in this study.

References

Acharyya, R. 2023. "Evaluation of Overall Response of Driven Pile in Multi-Layered Soil." *Transportation Infrastructure Geotechnology*. https://doi.org/10.1007/s40515-023-00354-7.

Alawneh, A. S., and A. A. Sharo. 2020. "Estimation of Long-Term Set-Up of Driven Piles in Sand." *Geomechanics and Geoengineering* 15 (4): 281–296. https://doi.org/10.1080/17486025.2019.1641630.

Ali, M. M., M. R. Selamat, S. S. Yii, and W. K. Ng. 2011. "On the Study of Pile Driving Formula Based on Blow Counts." *Geotechnical and Geological Engineering* 29 (3): 351–361. https://doi.org/10.1007/s10706-010-9381-x.

Bandyopadhyay, K., K. Das, S. Nandi, and A. Halder. 2022. "Dilatometer —An in situ Soil Exploration Tool for Problematic Ground Conditions vis-à-vis for Economizing Construction Activities." *Indian Geotechnical Journal* 52 (5): 1155–1170. https://doi.org/10.1007/s40098-022-00655-7.

Bandyopadhyay, K., A. Halder, S. Nandi, B. Koley, and S. Saraswati. 2021. "West Bengal." In *Geotechnical Characteristics of Soils and Rocks of India*, edited by Sanjay Kumar Shukla, 695–718. London: CRC Press.

Bowels, E. J. 1997. *Foundation Analysis and Design*. 5th ed. Singapore: Tata McGraw Hill Companies, Inc.

Bryson, S., and H. El Naggar. 2013. "Evaluation of the Efficiency of Different Ground Improvement Techniques." *Proceeding of the 18th International Conference on Soil Mechanics and Geotechnical Engineering*, Paris.

Das, K., S. Nandi, S. Chattaraj, A. Halder, and W. Sadhukhan. 2022. "Estimation of Subsoil Parameters and Settlement of Foundation for a Project in Kolkata Based on CPT, DMT." *Journal of Physics: Conference Series* 2286 (1): 012026. https://doi.org/10.1088/1742-6596/2286/1/012026.

Govindaraju, L., and S. Bhattacharya. 2012. "Site-Specific Earthquake Response Study for Hazard Assessment in Kolkata City, India." *Natural Hazards* 61 (3): 943–965. https://doi.org/10.1007/s11069-011-9940-3.

Halder, A., K. Das, S. Nandi, and K. Bandyopadhyay. 2022. "A Comparative Study on Liquefaction Assessment of Rajarhat Area of Kolkata by using Different Approaches." In *Cone Penetration Testing*, edited by Guido Gottardi and Laura Tonni, 955–960. London: CRC Press.

Hanna, T. H. 1967. "The Measurement of Pore Water Pressures Adjacent to a Driven Pile." *Canadian Geotechnical Journal* 4 (3): 313–325. https://doi.org/10.1139/t67-053.

Hashash, Y. M. A., M. I. Musgrove, J. A. Harmon, O. Ilhan, G. Xing, O. Numanoglu, D. R. Groholski, C. A. Phillips, and D. Park. 2020. *DEEPSOIL 7.0, user Manual*. Urbana, IL: Board of Trustees of University of Illinois at Urbana-Champaign.

Indian Standard. 2006. "Code of Practice for Design and Construction of Foundations in Soils: General Requirements." *IS 1904 -1986*.

Indian Standard. 2016. "Criteria for Earthquake Resistance Design of Structures, is 1893 (Part I)."

IS (Indian Standard) 6426. 1972. *Code of Practice for Specification for Pile Driving Hammer*. New Delhi, India: Bureau of Indian Standards.

Kaushik, Bandyopadhyay, and Sunanda Bhattacharjee. 2015. "Comparative Study of Sub-Soil Profiles Obtained by SDMT and SPT Tests and Subsequent Determination of Settlement of Post-Earthquake Condition." *Japanese Geotechnical Society Special Publication* 3 (2): 90–96.

Klammler, H., M. McVay, R. Herrera, and P. Lai. 2013. "Reliability Based Design of Driven Pile Groups Using Combination of Pile Driving Equations and High Strain Dynamic Pile Monitoring." *Structural Safety* 45:10–17. https://doi.org/10.1016/j.strusafe.2013.07.009.

Mabsout, M. E., L. C. Reese, and J. L. Tassoulas. 1995. "Study of Pile Driving by Finite-Element Method." *Journal of Geotechnical Engineering* 121 (7): 535–543. https://doi.org/10.1061/(ASCE)0733-9410(1995)121:7(535).

Marchetti, D. M. T. "Home Page." https://www.marchetti-dmt.it/.

Marchetti, S. 1980. "In situ Tests by Flat Dilatometer." *Journal of the Geotechnical Engineering Division* 106 (3): 299–321. https://doi.org/10.1061/AJGEB6.0000934.

Marchetti, S. 1997. "The Flat Dilatometer: Design Applications." *Proceeding 3rd International Geotechnical Engineering Conference*, 421–448. Cairo City.

Marchetti, S., P. Monaco, G. Totani, and M. Calabrese. 2001. *The Flat Dilatometer Test (DMT) in Soil Investigations–A Report by the ISSMGE Committee TC16*. Washington DC: Proceedings In Situation.

Monaco, P., S. Marchetti, G. Totani, and M. Calabrese. 2005. "Sand Liquefiability Assessment by Flat Dilatometer Test (DMT)." *Proceedings of the 16th International Conference on Soil Mechanics and Geotechnical Engineering*, 2693–2698. Osaka, Japan: IOS Press.

NEIC (National Earthquake Information Center). https://www.usgs.gov/programs/earthquake-hazards/earthquakes.

Ravichandran, N., T. Vickneswaran, S. Marathe, and V. S. Jella. 2021. "Numerical Analysis of Settlement Response of Shallow Footing Subjected to Heavy Rainfall and Flood Events." *International Journal of Geosciences* 12 (2): 138–158. https://doi.org/10.4236/ijg.2021.122009.

Salahudeen, A. B., and J. A. Sadeeq. 2017. "Investigation of Shallow Foundation Soil Bearing Capacity and Settlement Characteristics of Minna City Centre Development Site using Plaxis 2D Software and Empirical Formulations." *Nigerian Journal of Technology* 36 (3): 663–670. https://doi.org/10.4314/njt.v36i3.1.

Shiuly, A., and J. P. Narayan. 2012. "Deterministic seismic microzonation of Kolkata city." *Natural Hazards* 60 (2): 223–240. https://doi.org/10.1007/s11069-011-0004-5.

Vilas, M. K., and K. Moniuddin. 2015. "Finite Element Analysis of Soil Bearing Capacity using Plaxis." *International Journal of Engineering Research & Technology* 4 (6). https://doi.org/10.17577/IJERTV4IS060813.

Yin, J., X. Bai, N. Yan, S. Sang, L. Cui, J. Liu, and M. Zhang. 2023. "Dynamic Damage Characteristics of Mudstone Around Hammer Driven Pile and Evaluation of Pile Bearing Capacity." *Soil Dynamics and Earthquake Engineering* 167:107789. https://doi.org/10.1016/j.soildyn.2023.107789.

Zhang, L. M., L. M. Shek, H. W. Pang, and C. F. Pang. 2006. "Knowledge-Based Design and Construction of Driven Piles." *Proceedings of the Institution of Civil Engineers - Geotechnical*

Engineering 159 (3): 177–185. https://doi.org/10.1680/geng.2006.159.3.177.

Zhang, L., W. H. Tang, and C. W. Ng. 2001. "Reliability of Axially Loaded Driven Pile Groups." *Journal of Geotechnical and Geoenvironmental Engineering* 127 (12): 1051–1060. https://doi.org/10.1061/(ASCE)1090-0241(2001)127:12(1051).

Zhang, Y., J. Yin, X. Bai, L. Cui, S. Sang, J. Liu, N. Yan, and M. Zhang. 2023. "Study on Damage Constitutive Relationship of Mudstone Affected by Dynamic Pile Driving." *Soil Dynamics and Earthquake Engineering* 164:107653. https://doi.org/10.1016/j.soildyn.2022.107653.

Zhao, C. Y., W. M. Leng, and G. Y. Zheng. 2013. "Calculation and Analysis for the Time-Dependency of Settlement of the Single-Driven Pile in Double-Layered Soft Clay." *Applied Clay Science* 79:8–12. https://doi.org/10.1016/j.clay.2013.02.022.

Appendix A

Calculation of Modulus of Subgrade Reaction

k_s calculation for DMT6 test point
Raft foundation (L x B) = 24.0 m× 52.0 m
Depth of the foundation (D) = 5.25 m
*E*of soil upto average depth 10.20 m = 35370 kPa
μ = 0.3

$$Es' = \left(\frac{1-\mu^2}{E_s}\right) = 2.5728\text{E} - 05\,\text{kPa}$$

k_s for Center
H/B' = 10, L/B = 2.167, D/B = 0.219, as B' = B/2, H = 5B [27]

$$\text{I}_1 = 0.666, \text{I2} = 0.036, Is = I_1 + \left(\frac{1-2\mu}{1-\mu}\right)I_2 = 0.687\,[27]$$

I_F = 0.841 [11]
$k_s = \frac{1}{mBE_sI_sI_F}$ = 1402.24 (kN/m^3)
k_s for Corner
H/B' = 5, L/B = 2.167, D/B = 0.219, as B' = B, H = 5B [27]

$$\text{I}_1 = 0.544, \text{I2} = 0.066, I_s = I_1 + \left(\frac{1-2\mu}{1-\mu}\right)I_2 = 0.582\,[27]$$

I_F = 0.841 [27]

$$k_s = \frac{1}{\text{mBE}_\text{s}\text{I}_\text{s}\text{I}_\text{F}} = 3310.705\,\left(\text{kN/m}^3\right)$$

$$k_s \text{ Avg.} = \left(\frac{4\left(k_{s,corner}\right) + k_{s,corner}}{5}\right)(L \times B) = 2226348.523\,(\text{kN/m})$$

k_s calculation for DMT´3 test point
Raft foundation $(L \times B)$ = 24.0m × 52.0 m
Depth of the foundation (D) = 5.25 m
*E*of soil upto average depth 10.20 m = 52560 kPa
μ = 0.3

$$Es' = \left(\frac{1-\mu^2}{\text{E}_\text{s}}\right) = 1.73135E - 05\,\text{kPa}$$

k_s for Center
H/B' = 10, L/B = 2.167, D/B = 0.219, as B' = B/2, H = 5B [27]

$$\text{I}_1 = 0.666, \text{I}_2 = 0.036, Is = I_1 + \left(\frac{1-2\mu}{1-\mu}\right)I_2 = 0.687[27]$$

I_F = 0.841 [27]

$$k_s = \frac{1}{\text{mBE}_\text{s}\text{I}_\text{s}\text{I}_\text{F}} = 2038.736\left(\text{kN/m}^3\right)$$

k_s for Corner
H/B' = 5, L/B = 2.167, D/B = 0.219, as B' = B, H = 5B [27]

$$\text{I}_1 = 0.544, \text{I2} = 0.066, Is = I_1 + \left(\frac{1-2\mu}{1-\mu}\right)I_2 = 0.582[27]$$

I_F = 0.841 [27]

$$k_s = \frac{1}{\text{mBE}_\text{s}\text{I}_\text{s}\text{I}_\text{F}} = 4919.724\left(\text{kN/m}^3\right)$$

$$ks_{\text{Avg.}} = \left(\frac{4\left(k_{s,corner}\right) + k_{s,corner}}{5}\right)(L \times B) = 3308365.235\,(\text{kN/m})$$